photonics

MDPI

Article

Enhanced Performance of a Cascaded Receiver Consisting of a DNN-Based Waveform-to-Symbol Converter and Modified NN-Based DD-LMS in CAP Underwater VLC System

Xianhao Lin [1,2,3], Fangchen Hu [1,2,3] and Nan Chi [1,2,3,*]

[1] Key Laboratory for Information Science of Electromagnetic Waves (MoE), Fudan University, Shanghai 200433, China
[2] Shanghai Engineering Research Center of Low-Earth-Orbit Satellite Communication and Applications, Shanghai 200433, China
[3] Shanghai Collaborative Innovation Center of Low-Earth-Orbit Satellite Communication Technology, Shanghai 200433, China
* Correspondence: nanchi@fudan.edu.cn

Abstract: Underwater visible light communication (UVLC) based on LEDs has become a competitive candidate, which is able to provide high data rates, low latency and low cost for next-generation wireless communication technologies. However, it is still challenging to achieve high-speed communication because of bottleneck problems such as bandwidth limitation and linear and nonlinear distortions. Traditional Deep-learning Neural Network (DNN)-based waveform-to-symbol converter is verified to be an effective method to alleviate them, but impractical due to high complexity. To achieve a better tradeoff between communication performance and computation complexity, a cascaded receiver consisting of a DNN-based waveform-to-symbol converter and modified Neural Network (NN)-based decision-directed least mean square (DD-LMS) is then innovatively proposed. With fewer taps and nodes than the traditional converter, the front-stage converter could mitigate the majority of Inter-Symbol Interference (ISI) and signal nonlinear distortions. Then modified NN-based DD-LMS is cascaded to improve communication performance by reducing phase offset, making received constellation points more concentrated and closer to standard constellation points. Compared with the traditional converter, the cascaded receiver could achieve 89.6% of signal Vpp dynamic range with 12.4% of complexity in the 64APSK UVLC system. Moreover, the ratio of signal Vpp dynamic range and total trainable parameters is 1.24×10^{-1} mV, while that of the traditional converter is 1.95×10^{-2} mV. The cascaded receiver used in 64APSK UVLC systems is experimentally verified to achieve enhanced performance, thus as a promising scheme for future high-speed underwater VLC.

Keywords: underwater visible light communication (UVLC); neural network (NN); waveform-to-symbol converter; DD-LMS

Citation: Lin, X.; Hu, F.; Chi, N. Enhanced Performance of a Cascaded Receiver Consisting of a DNN-Based Waveform-to-Symbol Converter and Modified NN-Based DD-LMS in CAP Underwater VLC System. *Photonics* **2023**, *10*, 79. https://doi.org/10.3390/photonics10010079

Received: 10 December 2022
Revised: 5 January 2023
Accepted: 5 January 2023
Published: 10 January 2023

1. Introduction

With the exploration of marine resources and the increase of human underwater activities, the demand for efficient underwater communication has increased significantly. At present, the most widely applied means of underwater wireless communication is acoustic technology, which still suffers from low data rate, high signal attenuation, high latency and severe multipath effect. As for radio frequency (RF) which is commonly used in our daily life, it is not very suitable for underwater communication due to the high attenuation of RF waves in seawater. Another way is utilizing fiber optic to implement long-range and high-speed underwater communication. However, it is not flexible enough for increasingly diverse underwater applications because of the requirement of a physical cable connection between transmitters and receivers. Therefore, underwater visible light

communication (UVLC) has aroused wild attention and is considered an alternative or complement to the underwater communication technologies mentioned above [1–3].

Visible light communication (VLC) is an emerging wireless communication technology with several advantages such as large transmission capacity, high security, low cost, anti-electromagnetic interference and license-free [4–6]. Considering the relatively low attenuation window of seawater in the blue-green portion of the electromagnetic spectrum, VLC has great potential to provide a high data rate and low latency within a short range [1,2]. There are two kinds of commonly used VLC transmitters, which are based on laser diodes (LDs) and light-emitting diodes (LEDs). LDs enable longer-range transmission in point-to-point scenarios due to their high power density but require strict alignment between transmitters and receivers. Compared with LDs, LEDs have a larger divergence angle, which allows for more short-range applications, including point-to-point and point-to-multipoint scenarios [7]. In this paper, we focus on UVLC systems based on LEDs which have become a promising candidate for underwater communication.

Despite the many significant advantages of UVLC systems based on LEDs mentioned above, the bottleneck problems it faces cannot be ignored. The limited bandwidth of LEDs, various noises, and linear and nonlinear distortions largely restrict the communication performance of UVLC systems [6]. The modulation bandwidth of commercially available LEDs is usually several megahertz (MHz) [8], which has become one of the main factors limiting the development of high-speed VLC systems. Due to the bandwidth limitation of LEDs and other optoelectronic devices, the received signals suffer from serious linear distortion, thus interfering with the correct demodulation and decoding. When the bandwidth of the transmission signals exceeds the effective bandwidth of VLC systems, the bandwidth limitation behaves as a strong low-pass filter, which will compress the signal spectrum, resulting in serious inter-symbol interference (ISI). Furthermore, the signals' nonlinear effects will severely deteriorate communication performance, which results from the nonlinearity of devices' optoelectronic characteristics, distortions caused by amplifiers and so on. When the transmitting power is very high and the channel is complex, nonlinearity will become the main challenge restricting the systems' performance, especially for underwater applications, which usually require considerable transmitting power.

To alleviate these bottleneck problems, advanced modulation formats are proposed, including carrier-less amplitude and phase (CAP) modulation [9], adaptive bit loading Orthogonal Frequency Division Multiplexing (OFDM) [10] and Nyquist single carrier (N-SC) modulation [11]. To further improve communication performance, Geometrically-shaping (GS) technology [12] was proposed to increase Euclidean distance between the constellation points and decrease Peak-to-Average Power Ratio (PAPR) by optimizing the constellation distribution. For example, APSK, which is one kind of GS constellation point, has been adopted by the second-generation digital video broadcasting specification for satellite (DVB-S2) and approved by the consultative committee for space data systems (CCSDS) [13,14]. Besides, post-equalization algorithms based on advanced digital signal processing (DSP) are proposed to mitigate linear and nonlinear distortions. At present, linear time-frequency domain equalization technology based on least mean square (LMS) [15], recursive least square (RLS) [16], direct decision least mean square (DD-LMS), zero-forcing [17] and other algorithms have been utilized in VLC systems, effectively eliminating linear distortion. In terms of nonlinear distortions, a series of nonlinear equalizers have also been proposed, such as Volterra series-based and Polynomial based algorithms [18].

Recently, artificial intelligence algorithms, especially neural networks (NN), are emerging as effective techniques to deal with nonlinear problems. Due to NN's universal approximation theorem, it is commonly used as a post-equalization algorithm in VLC systems. In [19], a Gaussian kernel-aided deep neural network (GK-DNN) equalizer was utilized to compensate for the high nonlinear distortion of underwater PAM8 VLC channels. In [20], Lu et al. proposed a memory-controlled deep LSTM neural network post-equalizer for PAM-based VLC systems. In [21], a nonlinear resilient learning post-equalizer named

TFDNet was proposed. It exploits time-frequency image analysis, which considers the time and frequency domains simultaneously and is effective in tackling nonlinear distortions in UVLC systems. Except for equalizers, DNNs were recently used as a waveform to symbol converter, which could replace conventional demodulation, post-equalization, and down-sampling at the receiving end. In [22], a sparse data-to-symbol neural network (SDSNN) receiver is proposed for UVLC based on nonorthogonal multi-band CAP to mitigate ISI and inter-channel interference (ICI). In [23], a Neural-network-based waveform to symbol converter (NNWSC) can directly convert the received multiband CAP waveform into quadrature amplitude modulation (QAM) symbols to simultaneously handle the ISI and ICI in a fiber-mmWave system. In [24], a DNN-based waveform to symbol decoder with three hidden layers was utilized in UVLC systems and achieved better communication performance than a traditional receiver. Moreover, neural networks are now becoming more and more popular in channel estimation [25] and end-to-end learning [26,27].

In this paper, we first construct and optimize a traditional DNN-based waveform-to-symbol converter [24] to replace conventional demodulation, down-sampling and post-equalization at the receiving end in 64QAM and 64APSK UVLC systems based on CAP modulation. It is regarded as a benchmark that could increase signal Vpp dynamic range by 104% (from 250 mV to 511 mV) for 64APSK and 181% (from 180 mV to 506 mV) for 64QAM with 7% FEC of 3.8×10^{-3} as a BER threshold, compared with traditional CAP receiver. However, it comes at the cost of the high complexity of 26,210 trainable parameters. To achieve a better tradeoff between communication performance and computation complexity which is represented by total trainable parameters, we then innovatively propose a cascaded receiver consisting of a DNN-based waveform-to-symbol converter and modified NN-based DD-LMS. With fewer taps and nodes than the traditional converter, the front-stage converter could still mitigate the majority of ISI and signal distortions. Then modified NN-based DD-LMS is cascaded to improve communication performance by reducing phase offset, making received constellation points more concentrated and closer to standard constellation points. Compared with the traditional converter, the cascaded receiver could achieve 89.6% of signal Vpp dynamic range with 12.4% of complexity in the 64APSK UVLC system. Moreover, the ratio of signal Vpp dynamic range and total trainable parameters is 1.24×10^{-1} mV, while that of the traditional converter is 1.95×10^{-2} mV. It is experimentally validated that the cascaded receiver using 64APSK is an effective method to enhance the performance of UVLC systems based on CAP modulation.

2. Principle

2.1. Principle of CAP Modulation and Conventional CAP Receiver

CAP modulation is one kind of advanced multi-dimension and multi-level modulation format, which achieves a high data rate and high spectral efficiency with limited bandwidth [28,29]. CAP modulation can adopt any order m-QAM signal for flexible coding to achieve high-order modulation, and FIR filters are used for pulse shaping, so its signal bandwidth is close to the minimum bandwidth of Nyquist theory. Compared with traditional QAM and OFDM modulation, electrical or optical complex-to-real-value conversion and discrete Fourier transform (DFT) are no longer required, which means that the system complexity can be greatly reduced. Therefore, it is a promising modulation scheme for bandwidth-limited and low-complexity required UVLC systems.

At the transmitting end, the original bit sequence is firstly mapped to M-order complex symbols. When using GS technology, the mapping methods are different, thus obtaining constellation points of different shapes. For example, 64QAM has square constellation points, while 64APSK has four circles. Then, complex symbols are up-sampled according to the minimum number of samples per symbol, which avoids spectrum aliasing. After that, the symbols are separated into the in-phase and quadrature components, which are represented by $s_I(t)$ and $s_Q(t)$ respectively. Finally, they are sent into a pair of orthogonal shaping filters and added together to generate CAP-modulated signals that will be con-

verted into analog signals through a digital-to-analog converter (DAC). The signals can be expressed as

$$s(t) = s_I(t) \otimes f_I(t) - s_Q(t) \otimes f_Q(t) \tag{1}$$

Here, $\otimes$ represents a convolution operation. $f_I(t)$ and $f_Q(t)$ are the corresponding impulse response of orthogonal shaping filters in the time domain, which can be expressed as

$$\begin{cases} f_I(t) = \mathrm{g}(t)\cos(2\pi f_c t) \\ f_Q(t) = \mathrm{g}(t)\sin(2\pi f_c t) \end{cases} \tag{2}$$

In Formula (2), f_c is the central frequency of shaping filters, which can be expressed as $f_c = (1+\alpha)/2T + \Delta f$. T, Δf, and α are the symbol period, frequency offset and roll-off coefficient, respectively. $\mathrm{g}(t)$ is baseband impulse response which is usually root raised cosine filter. It can be expressed as

$$\mathrm{g}(t) = \frac{T\sin[\pi(1-\alpha)t/T] + 4\alpha t\cos[\pi(1+\alpha)t/T]}{\pi t\left[1-(1-(4\alpha t/T))^2\right]} \tag{3}$$

At the receiving end, the received CAP waveform suffers from severe distortions due to serious linear or nonlinear damage and noise interference. So linear or nonlinear waveform-level equalization algorithms are usually utilized for a received signal after being sampled and quantified by an oscilloscope, such as LMS [15] or Volterra series-based algorithms [18] and so on. Then the signals pass through a pair of matched filters to obtain the in-phase and quadrature components, which can be expressed as

$$\begin{cases} r_I(t) = r(t) \otimes m_I(t) \\ r_Q(t) = r(t) \otimes m_Q(t) \end{cases} \tag{4}$$

Here, $m_I(t) = f_I(-t)$ and $m_Q(t) = f_Q(-t)$ are corresponding impulse response of the corresponding matched filters. I and Q signal are combined with being complex symbols after matched filtering and down-sampling, which are actually received constellation points. To further mitigate inter-symbol interference (ISI) and linear or nonlinear distortions, symbol-level post-equalizations are widely applied, including zero-forcing, LMS, DD-LMS, RLS, Volterra series and even neural network-based post equalization algorithms mentioned above. Finally, the original bit data can be retrieved from de-mapping.

2.2. Principle of a Cascaded Receiver Consisting of a DNN-Based Waveform-to-Symbol Converter and Modified NN-Based DD-LMS

Thanks to the artificial neural network's universal approximation theorem, it is feasible to convert the received signal waveform with severe ISI and distortions into complex symbols or constellation points directly by using a well-trained neural network [23]. It is called a waveform-to-symbol converter that replaces conventional waveform-level equalization, matched filtering, down-sampling, and symbol-level post-equalization. Compared with conventional multi-stage processing at the receiving end, a DNN-based waveform-to-symbol converter optimizes the receiver as a whole and achieves better performance due to the powerful ability of a neural network to find out implicit relationships between received waveforms and symbols [24]. However, the converter must be of large enough complexity to convert received waveforms into symbols perfectly. To achieve a better tradeoff between communication performance and computation complexity, a cascaded receiver consisting of a DNN-based waveform-to-symbol converter and modified NN-based DD-LMS is proposed in this paper. Although with fewer taps and nodes than traditional converter [24], we will optimize in this paper the front-stage DNN-based waveform-to-symbol converter could mitigate the majority of ISI and signal nonlinear distortions. Then modified NN-based DD-LMS is cascaded to eliminate remaining ISI and distortions and improve signal quality even further. Thus, the cascaded receiver could achieve excellent communication performance with relatively low complexity.

The schematic of the proposed algorithm is shown in Figure 1. At the transmitter end, an original pseudorandom binary sequence is generated and then mapped to 64QAM or 64APSK complex symbols using GS technology. The constellation points of 64QAM are square, while those of 64APSK consists of four rings. These symbols are converted to transmitted waveforms after CAP modulation. After traveling from transmitter to receiver, the received signals have experienced severe inter-symbol interference (ISI) and distortions due to bandwidth limitation of LED, various noises, and linear and nonlinear damages. The transmitted and received signals are displayed in Figure 1, where the waveform distortions can be observed both in the time domain and frequency domain, respectively.

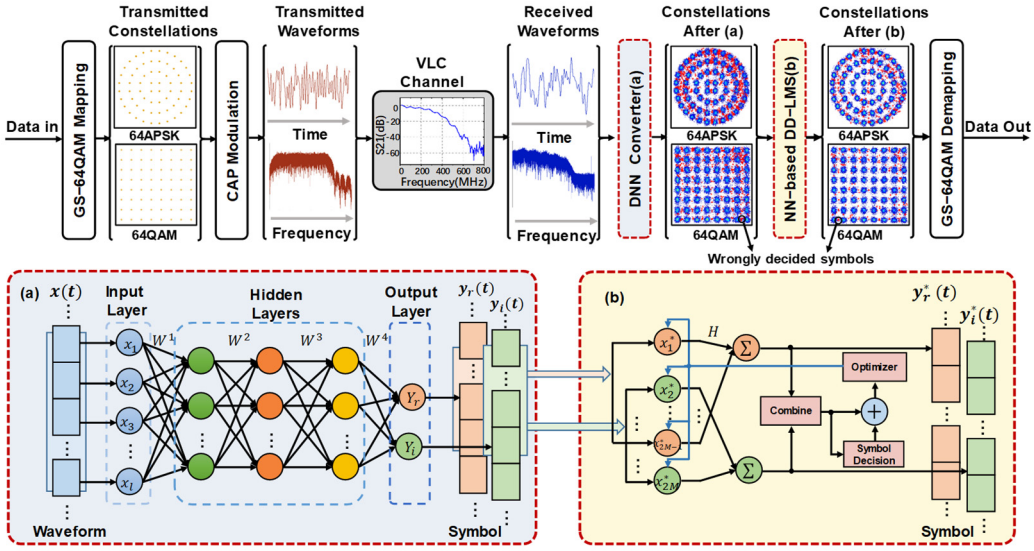

Figure 1. The schematic diagram of the UVLC system using the cascaded receiver. (**a**) shows the details of the front-stage DNN-based waveform-to-symbol converter at the front stage. (**b**) shows the details of the modified NN-based DD-LMS at the rear stage.

The received signals are then sent into a DNN-based waveform-to-symbol converter, whose structure is shown in Figure 1a. It consists of one input layer with N nodes, three hidden layers with n_1, n_2, and n_3 nodes, respectively and one output layer with two nodes that correspond to the real and imaginary parts of the output. Considering inter-symbol interference, a sliding window is applied to received signals $x(t)$. The j^{th} slice can be expressed as:

$$X(j) = \left\{ x\left(j - \frac{l-1}{2}\right), \ldots, x(j-1), x(j), x(j+1), \ldots, x\left(j + \frac{l-1}{2}\right) \right\} \tag{5}$$

where l is an odd number that represents the length of the sliding window. The step size of the sliding window equals the number of up-sampling. For example, four times up-sampling is adopted in this paper, so the step size would be set as four. Then each slice will be calculated by three hidden layers in turns and connected to two output nodes to produce the real and imaginary parts, respectively. The j^{th} output can be expressed as:

$$y_{out}(j) = [y_r(j), y_i(j)]^T \tag{6}$$

where $y_r(j)$ and $y_i(j)$ denote the real and imaginary parts of j^{th} output. The relationship between input and output can be expressed as:

$$y_{out}(j) = W^4 f\left(W^3 f\left(W^2 f\left(W^1 f(X(j)) + b^1\right) + b^2\right) + b^3\right) + b^4 \tag{7}$$

where W^1, W^2, W^3 and W^4 represent the weight matrices for each layer respectively, b^1, b^2, b^3 and b^4 represent the bias, respectively. $f(\cdot)$ denotes the nonlinear activation function (AF) Tanh(·), which could be expressed as [30],

$$\mathrm{Tanh(x)} = \frac{e^x - e^{-x}}{e^x + e^{-x}} \tag{8}$$

After experiencing forward propagation, the minimum mean square error (MSE) is employed as the loss function to calculate the difference between the predicted symbols and transmitted symbols. The weight W and bias b can be obtained by the following Equation (9),

$$\mathrm{W,b} = \underset{W,b}{\mathrm{argmin}} \frac{1}{m} \sum_{j=1}^{m} ||\hat{y}(j) - y_{out}(j)||^2 \tag{9}$$

where, $\hat{y}(j)$ is the j^{th} transmitted symbol, and $y_{out}(j)$ is the corresponding predicted symbol; m is the number of all symbols in one batch. In this algorithm, we utilize Adam optimizer and ReduceLROnPlateau, which is a commonly used strategy to adjust the learning rate.

The constellation points of 64APSK and 64QAM after the DNN-based waveform-to-symbol converter are displayed in Figure 1. There are a lot of red points that represent the wrongly decided symbols due to remaining ISI, linear and nonlinear distortions. Then the real part $y_r(t)$ and imaginary part $y_i(t)$ of outputs are sent to the modified NN-based DD-LMS algorithm after two slide windows, respectively. The k^{th} input $X^*(k)$ of NN-based DD-LMS can be expressed as:

$$X^*(k) = \left[y_r\left(k - \frac{M-1}{2}\right), y_i\left(k - \frac{M-1}{2}\right), \ldots, y_r(k), y_i(k), \ldots, y_r\left(k + \frac{M-1}{2}\right), y_i\left(k + \frac{M-1}{2}\right) \right]^T \tag{10}$$

where M is the length of the sliding window on the real or imaginary part, and $2M$ is the input length NN-based DD-LMS. According to our experiments, the input length of 42 would be the best. Then input signals are multiplied by the weight matrix H and connected to two output nodes that correspond to the real part $y_r^*(k)$ and imaginary part $y_i^*(k)$ of output. The k^{th} output can be expressed as,

$$y_{out}^* = [y_r^*(k), y_i^*(k)]^T \tag{11}$$

Therefore, the relationship between input and output can be given by,

$$y_{out}^*(k) = HX^*(k) \tag{12}$$

At the same time, $y_r^*(k)$ and $y_i^*(k)$ would be combined as a complex symbol and then de-mapped according to the principle of minimum Euclidean distance. Here, the weight matrix H, which is a 2-by-$2M$, could be updated by calculating the difference between the output symbols and those obtained by de-mapping. An Adam optimizer is utilized for intelligent adjustment of the learning rate, which contributes to outperforming traditional DD-LMS. Notedly, modified NN-based DD-LMS is still a blind algorithm, which means the initialization of weight matrix H should be carefully considered. To start with, the intermediate input symbol will be chosen as output by setting the two middle elements of H($h_{1,M}$ and $h_{2,M+1}$) as 1 and others as 0. So, the initial weight matrix H is given by,

$$H = \begin{bmatrix} 0, \ldots, 1, 0, \ldots, 0 \\ 0, \ldots, 0, 1, \ldots, 0 \end{bmatrix}_{2 \times 2M} \tag{13}$$

As shown in Figure 1, the wrongly decided symbols have greatly decreased after the modified DD-LMS. Therefore, a cascaded receiver consisting of a DNN-based waveform-to-symbol converter and modified NN-based DD-LMS is proposed for UVLC systems.

3. Setup

Figure 2 presents the experimental setup of a UVLC system using different receivers. At the transmitting end, the input data is firstly mapped onto 64QAM or 64APSK using GS technology. Then the modulation format of CAP is adopted. In the traditional CAP encoder, the signals are up-sampled by four times to prevent the spectrum from aliasing. Then the I and Q components pass through a pair of orthogonal square root raised cosine (SRRC) filters after I/Q separation. The roll-off factor of SRRC is 0.205. The transmitted signals are generated by adding together these two IQ signals and normalization. Next, the digital signals are loaded into AWG (Tektronix AWG710) to convert to electrical signals. The signals then pass through a hardware pre-equalizer (Eq.) which is used to compensate for the frequency attenuation at high-frequency components [8]. After that, the signals are amplified by an electrical amplifier (ZHL-2-8-s+) and coupled with a DC current through the Bias Tee (Mini-Circuit ZFBT-4R2GW-FT+), which is used to drive the blue LED. Finally, LED converts the electrical signals into optical signals that will be collimated into parallel light by the lens. The light travels through a 1.2-m water tank and arrives at the receiver.

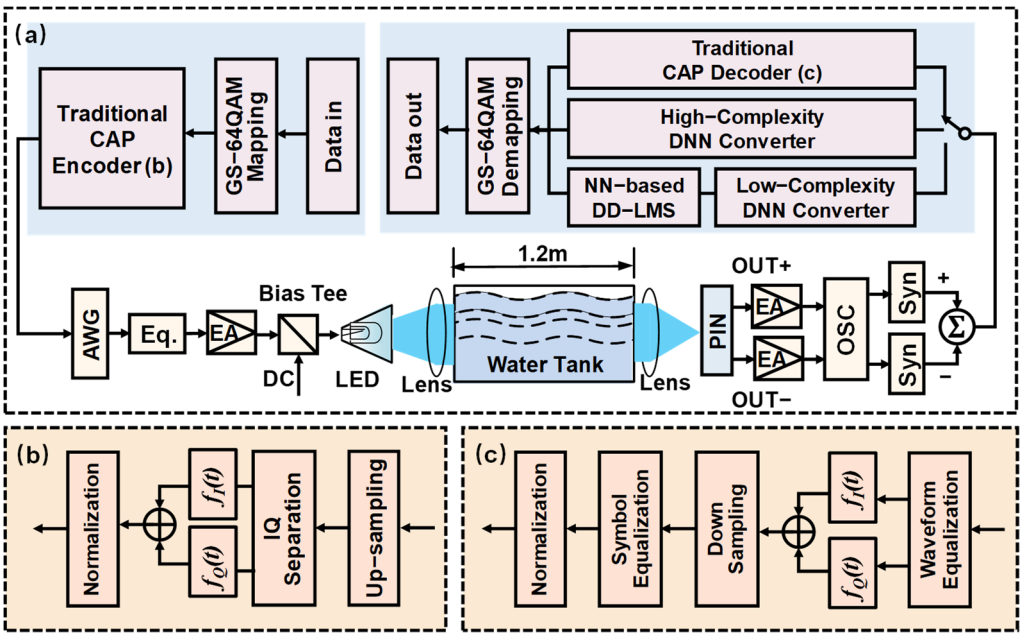

Figure 2. Experimental setup of Underwater VLC system using different receivers. (**a**) shows the overall setup of UVLC system in our experiments. (**b**) shows the details of traditional CAP encoder at the transmitting end. (**c**) shows the details of traditional CAP decoder at the receiving end.

At the receiving end, the optical signals are detected by a PIN photodiode (Hamamatsu 10784) which has a pair of differential outputs to suppress common mode noise. The differential signal streams are then amplified by EAs, acquired by OSC (DSO9404A) and synchronized to obtain received waveforms. Three different receivers are experimentally compared. The first one is the traditional CAP decoder, including waveform-level equalization, orthogonal filters, down-sampling, symbol-level equalization and normalization. The second one is a traditional DNN-based waveform-to-symbol converter (DNN converter) [24] that we optimize in this paper. It can find out the complex relationship between received waveforms and symbols with a high-complexity neural network. The last one is the proposed cascaded receiver consisting of a DNN converter with fewer taps or nodes and NN-based DD-LMS proposed in this paper. The DNN converter at the front stage could still handle the majority of ISI and nonlinear distortions. Then modified NN-based DD-LMS is cascaded to mitigate remaining ISI and distortions and further improve signal quality, thus achieving excellent performance with totally low complexity. Finally, the original data could be extracted from GS-64QAM de-mapping.

4. Experimental Results

In this section, we first construct and optimize a traditional DNN-based waveform-to-symbol converter (DNN converter) in 64APSK and 64QAM UVLC systems. Based on it, a cascaded receiver consisting of a DNN converter with fewer taps or nodes and an NN-based DD-LMS algorithm is experimentally analyzed in detail.

Figure 3 shows the relationship between the taps of traditional DNN-based waveform-to-symbol converter (DNN converter) and BER performance under different bias currents and signal Vpp, with 7% FEC of 3.8×10^{-3} as a BER threshold. Taps refer to the number of symbols corresponding to the input signal waveforms processed by the DNN converter at one time. Furthermore, the taps determine the number of inter-symbol interferences that the DNN converter can model. When the taps are less than 19, BER under different bias currents and signal, Vpp decreases rapidly as taps increase because it is not large enough to calculate the ISI. In this system, 19 taps allow a traditional DNN converter to achieve the best BER performance, which is clearly described in Figure 3. Because of the four times of upsampling, 19 taps mean that the input waveform length of the DNN converter is 76. However, as taps continue to increase, BER becomes worse. More taps lead to a more complex structure of DNN, requiring bigger data sets to train. Because of limited training data, overly complex networks cannot be trained better [19]. Therefore, there is a tradeoff between taps and the number of training data. The taps of 19 would be the best in our experiment. The constellation points of 19 under different bias currents and signal Vpp are displayed in Figure 3i–iv.

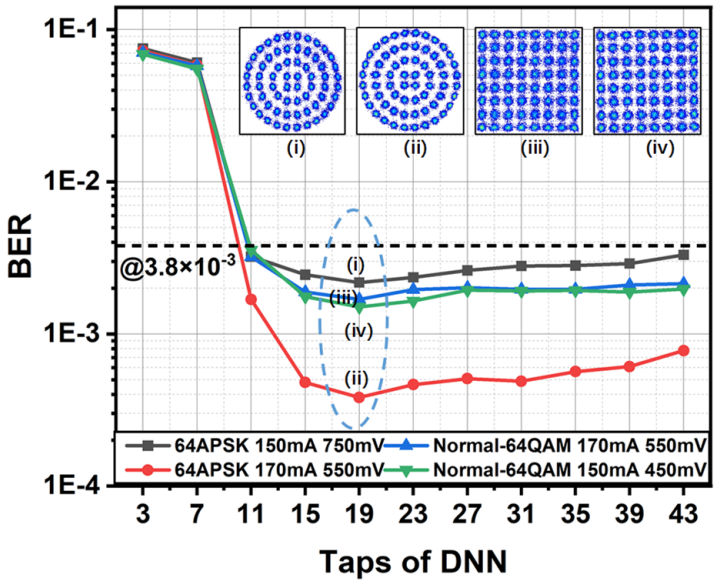

Figure 3. The relationship between BER performance and the taps of traditional DNN-based waveform-to-symbol converter under different bias currents and signal Vpp. (**i**–**iv**) show the constellation points of 19 taps under different bias currents and signal Vpp respectively.

Next, it is necessary to find the optimal structure of a traditional DNN converter. Figure 4a–c shows the relationship between BER performance and the number of hidden layers, nodes of each hidden layer, and the activation functions of traditional DNN converter under different signal Vpp, respectively. The bias current is fixed at 150 mA, and signal Vpp varies from 250 mV to 850 mV. In Figure 4a, the number of nodes in each hidden layer is set as 32. The DNN converters with different hidden layers ranging from 1 to 5 all outperform traditional CAP demodulation, especially in the high signal Vpp region. Thus, DNN-based waveform-to-symbol converters are experimentally demonstrated to be an effective scheme to improve the communication performance of UVLC systems. When the number of hidden layers increases from 1 to 3, the corresponding BER decreases. This is because the DNN converter requires a large enough complexity to fit the nonlinearity and

perfectly convert the signal waveforms into the corresponding symbols. As the number of hidden layers increases from 1 to 3, the DNN converter becomes more complex and fits the relationship between input and output more fully. However, as the number of hidden layers continues to increase from 3 to 5, the BER performance has not been further improved but has deteriorated somewhat. Because three hidden layers are sufficient to fit the nonlinear relationship between input and output, and no more layers are required. Instead, more hidden layers consume more computing resources and may lead to overfitting. Therefore, the number of hidden layers is chosen as 3. In Figure 4b, the DNN converter has three hidden layers with n_1, n_2, n_3 nodes respectively, so it is referred to as DNN (n_1, n_2, n_3). The BER performance of DNN (32, 32, 16), DNN (96, 64, 32), DNN (96, 96, 96) and DNN (128, 128, 128) are shown, compared with traditional CAP demodulation. DNN (96, 96, 96) achieves better performance than DNN (32, 32, 16) and DNN (96, 64, 32) due to greater complexity. Instead, DNN with too complex a structure easily leads to overfitting, which could be verified by DNN (128, 128, 128). In Figure 4c, the effects of different activation functions (Sigmoid, ReLU and Tanh) and no activation functions (None) have been investigated. The DNN converter with the activation function of Tanh has the best performance, then ReLU and Sigmoid. The DNN converter with no activation function has the worst performance that is similar to traditional CAP demodulation. Therefore, the DNN-based waveform-to-symbol converter we optimize has three hidden layers with 96, 96 and 96 nodes, and Tanh is employed as the activation function.

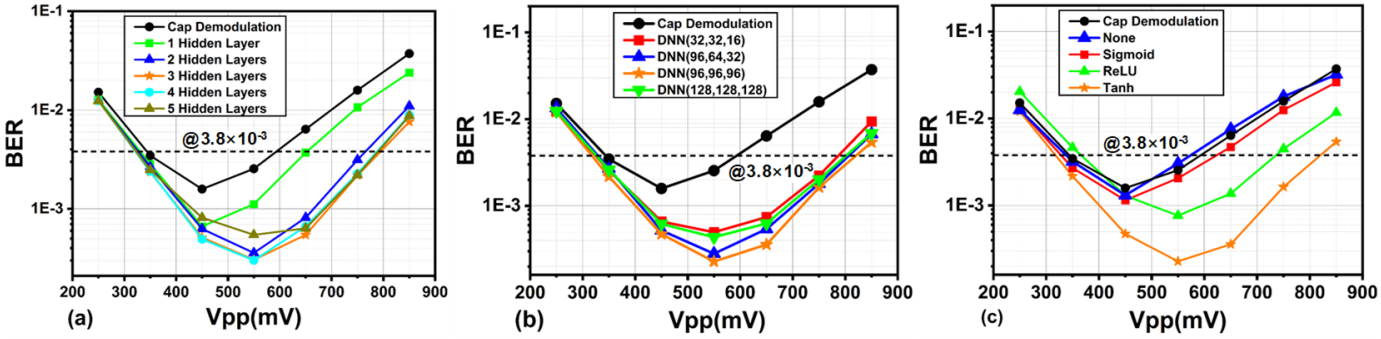

Figure 4. The relationship between BER performance and (**a**) the number of hidden layers; (**b**) nodes of each hidden layer; (**c**) the activation functions of traditional DNN converter under different signal Vpp.

Figure 5 presents the relationship between the BER performance of different taps and epochs during training, with 7a % FEC of 3.8×10^{-3} as a BER threshold. The bias current is 150 mA, and the signal Vpp is set as 550 mV. When the epoch is less than 200, the BER of the DNN converter decreases below the threshold rapidly. As the epoch continues to increase, BER drops slowly and converges gradually. It can be seen that the BER using a DNN converter with the taps of 19 is lower than 11 and 27 when training is finished, which is consistent with the results in Figure 3. Figure 5i–iv displays the constellation points obtained by the DNN converter with the taps of 19 when the epoch is 2, 50, 100, and 500, respectively. As the epoch increases, the constellation points become more and more clear and distinguishable.

Then the effects of the DNN converter on BER in 64QAM or 64APSK UVLC systems under different bias currents and signal Vpp are investigated, compared with traditional CAP demodulation. The results are presented in Figure 6, where the dynamic range of signal Vpp and bias current is circled by a black line of 2.0×10^{-3} FEC threshold. The bias current varies from 70 mA to 170 mA, and the signal Vpp varies from 250 mV to 750 mV. Comparing Figure 6a with Figure 6c, it can be seen that 64APSK systems work mainly in the higher current region where signals suffer from severe nonlinearity, which means that 64APSK is more advantageous to resist nonlinearity and it could obtain higher SNR in the circumstances of strong attenuation in UVLC systems. The DNN converter could

significantly extend the dynamic range both in 64APSK and 64QAM systems, especially in high signal Vpp region, because of its powerful ability to handle nonlinearity. However, in low signal Vpp region, BER performance using a DNN converter is similar to that using traditional CAP demodulation in 64APSK or 64QAM systems. This can be predicted because when signal Vpp is relatively low, noise plays a dominant role in the deterioration of communication performance, and the neural network is proven to be almost unable to handle it.

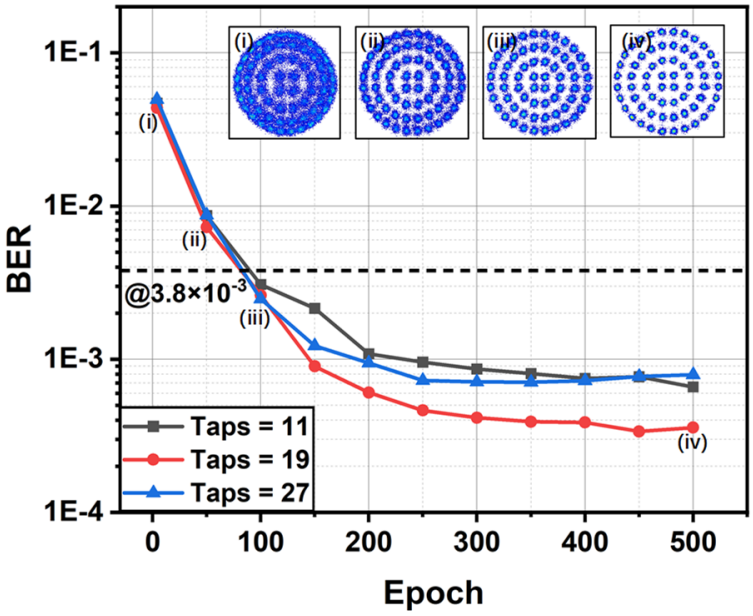

Figure 5. The relationship between BER performance of different taps and epoch during training. (**i–iv**) show the constellation points when epoch is 2, 50, 100 and 500, respectively.

In order to analyze the effects of the DNN converter, more specifically, the BER versus different signal Vpp for 64APSK and 64QAM UVLC systems under the bias current of 150 mA is demonstrated in Figure 7, compared with traditional CAP demodulation. In terms of traditional CAP demodulation (black curves in Figure 7a,b), the BER decreases as the increase of signal Vpp when it is smaller than 450 mV due to the enhancement of SNR. When it is larger than 450 mV, the BER versus signal Vpp has an opposite tendency because of nonlinear distortions. Thus, the signal Vpp dynamic range of signal Vpp is 250 mV for 64APSK and 180 mV for 64QAM with 7% FEC of 3.8×10^{-3}, respectively. The communication performance is significantly improved by using DNN converter (red curves in Figure 7a,b), as the signal Vpp dynamic range enlarges by 104% (from 250 mV to 511 mV) for 64APSK in Figure 7a and 181% (from 180 mV to 506 mV) for 64QAM in Figure 7b. Meanwhile, the Q factor of 950 mA biases current increases by 3.12 dB for 64APSK and 2.96 dB for 64QAM, compared with traditional CAP demodulation. It is experimentally verified that the DNN converter has obvious advantages over traditional CAP demodulation in the nonlinear region, thus more suitable for UVLC systems.

We also measured the Q factor for 64APSK and 64QAM UVLC systems at different bit rates under the optimal bias voltage and signaled Vpp with 7% FEC of 3.8×10^{-3} as a BER threshold. The performance of the DNN converter is in comparison with traditional CAP demodulation in Figure 8. As expected, the DNN converter could achieve greater communication capacity. To be specific, the highest bit rate is 3.23 Gb/s in the 64APSK system utilizing DNN converter and 3.09 Gb/s in 64QAM system, which is 125 Mb/s and 50 Mb/s faster than traditional CAP demodulation, respectively. 64APSK using the DNN converter is experimentally proved to be a promising scheme for future high-speed UVLC systems.

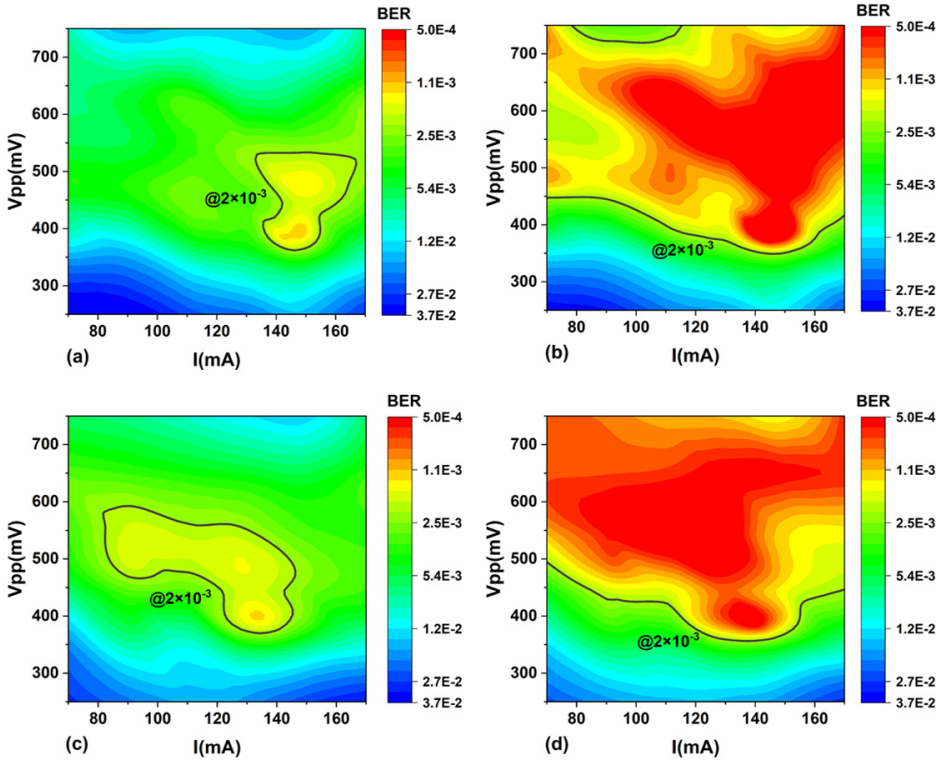

Figure 6. The contour of BER versus different bias currents and signal Vpp for (**a**) 64 APSK, traditional CAP demodulation; (**b**) 64APSK, DNN converter; (**c**) 64QAM, traditional CAP demodulation; (**d**) 64QAM, DNN converter.

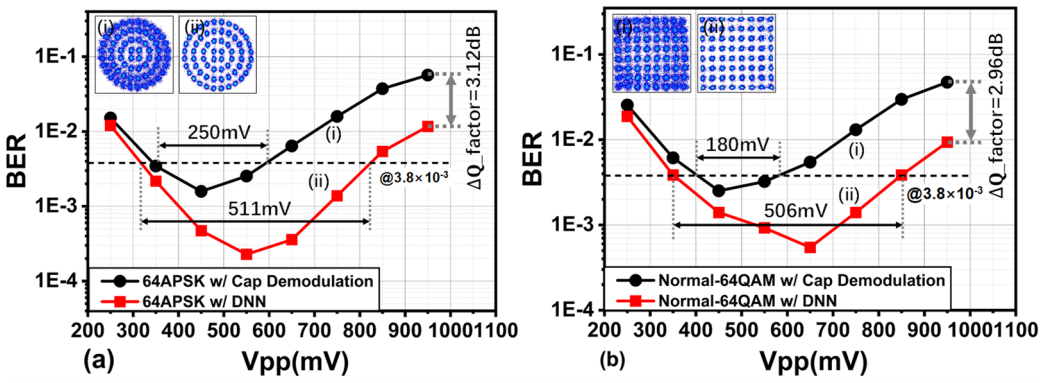

Figure 7. BER versus different Vpp for (**a**) 64APSK; (**b**) 64QAM UVLC systems.

At this point, the traditional DNN-based waveform-to-symbol converter we optimize is obtained. However, it is of high complexity to sustain the pressure of mitigating ISI, linear and nonlinear distortions, which is not expected for the implementation of UVLC systems. In order to achieve a better tradeoff between communication performance and computation complexity, we innovatively propose a cascaded receiver consisting of a DNN-based waveform-to-symbol converter and an NN-based DD-LMS algorithm. The DNN converter at the front stage is generated by appropriately reducing the taps or the nodes of hidden layers of the DNN converter we optimize above. It could still mitigate the majority of ISI and distortions of received signals. Then, a modified NN-based DD-LMS is utilized for further improving the quality of complex symbols (constellation points) produced by the DNN converter at the front stage. Thus, the algorithm could achieve similar performance to the traditional DNN converter we optimize but with much lower complexity.

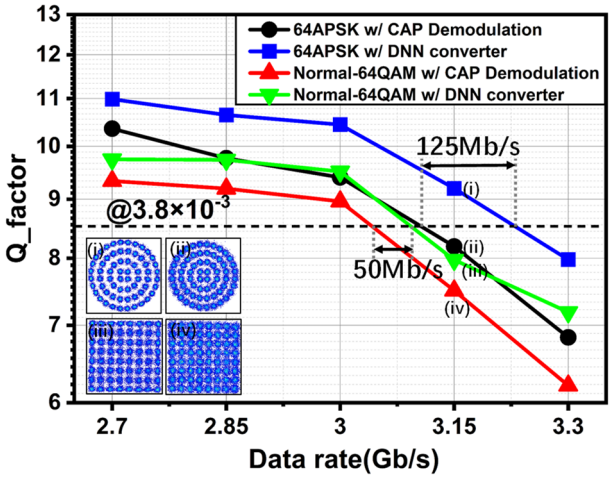

Figure 8. BER versus different Bit rate for 64APSK and 64QAM UVLC systems. (**i**,**ii**) show the constellation points of DNN converter and CAP demodulation in 64APSK UVLC systems when data rate is 3.15 Gb/s, respectively. (**iii**,**iv**) show the constellation points of DNN converter and CAP demodulation in 64QAM UVLC systems when data rate is 3.15 Gb/s, respectively.

In order to investigate the effects of modified NN-based DD-LMS on constellation points, we first pay attention to an important metric, which is phase offset. It is the average phase offset of each constellation point's class compared with standard constellation points. The results of 64APSK and 64QAM systems are shown in Figure 9a,b, respectively. The bias current is fixed at 150 mA, and signal Vpp varies from 250 mV to 950 mV. Based on the traditional DNN converter we optimize above, the front-stage DNN converter is obtained by reducing the taps from 19 to 11 and the nodes of three hidden layers from 96 to 32. As can be seen from Figure 9, the phase offsets after the front-stage DNN converter are still high due to remaining ISI and distortions. Fortunately, the phase offsets could be significantly reduced by modified NN-based DD-LMS, which indicates the improvement of communication performance. Figure 9i,ii show the movement vector of each constellation points' center after NN-based DD-LMS for 64APSK and 64QAM systems when signal Vpp is 550 mV, respectively.

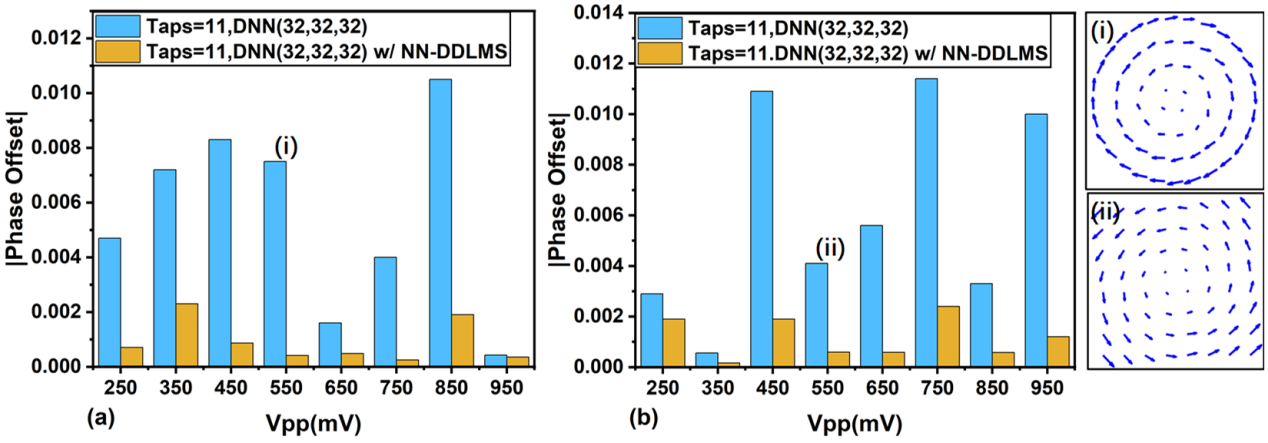

Figure 9. Phase Offset of DNN (32, 32, 32) with taps of 11 for (**a**) 64APSK; (**b**) 64QAM UVLC systems under different signal Vpp. (**i**,**ii**) show the movement vector of each constellation points' center after NN-based DD-LMS for 64APSK and 64QAM systems when signal Vpp is 550 mV, respectively.

In addition to phase offset, we measured the average distance between the received constellation points' center and standard constellation points. Moreover, a new metric named "Average Cluster Sum of Square" (ACSS) is proposed to represent how concentrated

the received constellation points are. The smaller ACSS is, the more concentrated the received constellation points are. ACSS can be expressed as,

$$\text{Average Cluster Sum of Square(ACSS)} = \frac{1}{64}\sum_{j=1}^{64}\left(\frac{1}{n_j}\sum_{i=1}^{n_j}||\boldsymbol{Y}_{ij}-\boldsymbol{u}_j||^2\right) \quad (14)$$

where $\boldsymbol{Y}_{ij}$ denotes the i^{th} point of j^{th} constellation points class and $\boldsymbol{u}_j$ denotes the center of j^{th} constellation points class. The results of DNN (32, 32, 32), DNN (64, 64, 64) and DNN (96, 96, 96) with the taps of 11 are shown in Figure 10. The average distances and ACSS under different signal Vpp for 64APSK UVLC systems are demonstrated in Figure 10a,b, respectively. It can be seen that after using NN-based DD-LMS, the average distance and ACSS both become smaller almost under every signal Vpp, which indicates that symbol decision would be more accurate after modified DD-LMS. The details of the 64 constellation points' class for the 64APSK system are shown in Figure 10i,ii, where blue and brown columns represent the results of the front-stage DNN converter with or without NN-based DD-LMS, respectively. The experimental results are similar for the 64QAM system, which are provided in Figure 10c,d.

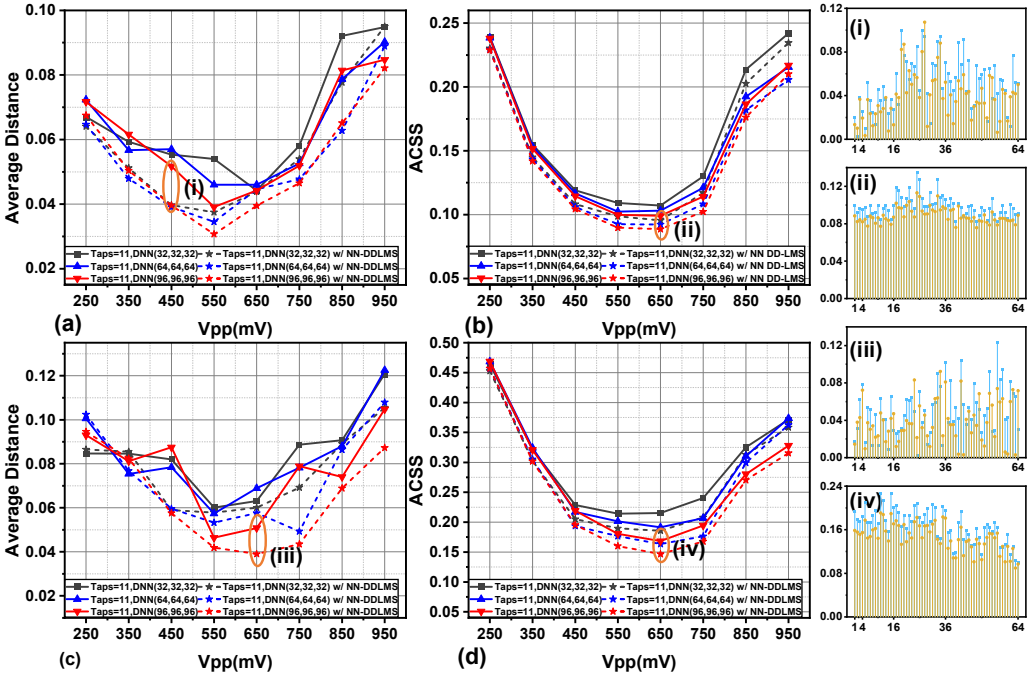

Figure 10. (**a**) The average distance between the center of received constellation points' class and standard constellation points for 64APSK systems; (**b**) ACSS for 64APSK systems; (**c**) the average distance for 64QAM systems; (**d**) ACSS for 64QAM systems.

In summary, NN-based DD-LMS could improve communication performance by reducing phase offset, making constellation points more concentrated and closer to standard constellation points. Then the communication performance of the cascaded receiver we proposed is presented in Figure 11a–d with 7% FEC of 3.8×10^{-3} as a BER threshold, compared with traditional CAP demodulation and typical DD-LMS. Figure 11a shows that in 64APSK UVLC systems, the BER of using a DNN converter is much lower than traditional CAP demodulation in the high-power region. The red line represents the traditional DNN converter we optimize, and it achieves the best communication performance. When reducing the taps from 19 to 11, the communication performance becomes worse due to remaining ISI and signal distortions, in which the dynamic range is 475 mV. After using typical DD-LMS or NN-based DD-LMS, BER performance is enhanced. Furthermore, using modified NN-based DD-LMS could achieve better performance than typical DD-

LMS due to the usage of Adam optimizer. In Figure 11b, cascaded receivers consisting of DNN converters with different complexity and NN-based DD-LMS are investigated in 64APSK systems. The traditional DNN converter we optimize has the largest dynamic range of 511 mV. When reducing the taps from 19 to 11, the dynamic range of the DNN converter with NN-based DD-LMS is 497 mV. Continuing to reduce the complexity, the BER performance is slightly worse. The dynamic range of signal Vpp is 481 mV for DNN (64, 64, 64) with NN-based DD-LMS and 458 mV for DNN (32, 32, 32) with NN-based DD-LMS. The trend is similar for 64QAM in Figure 11c,d.

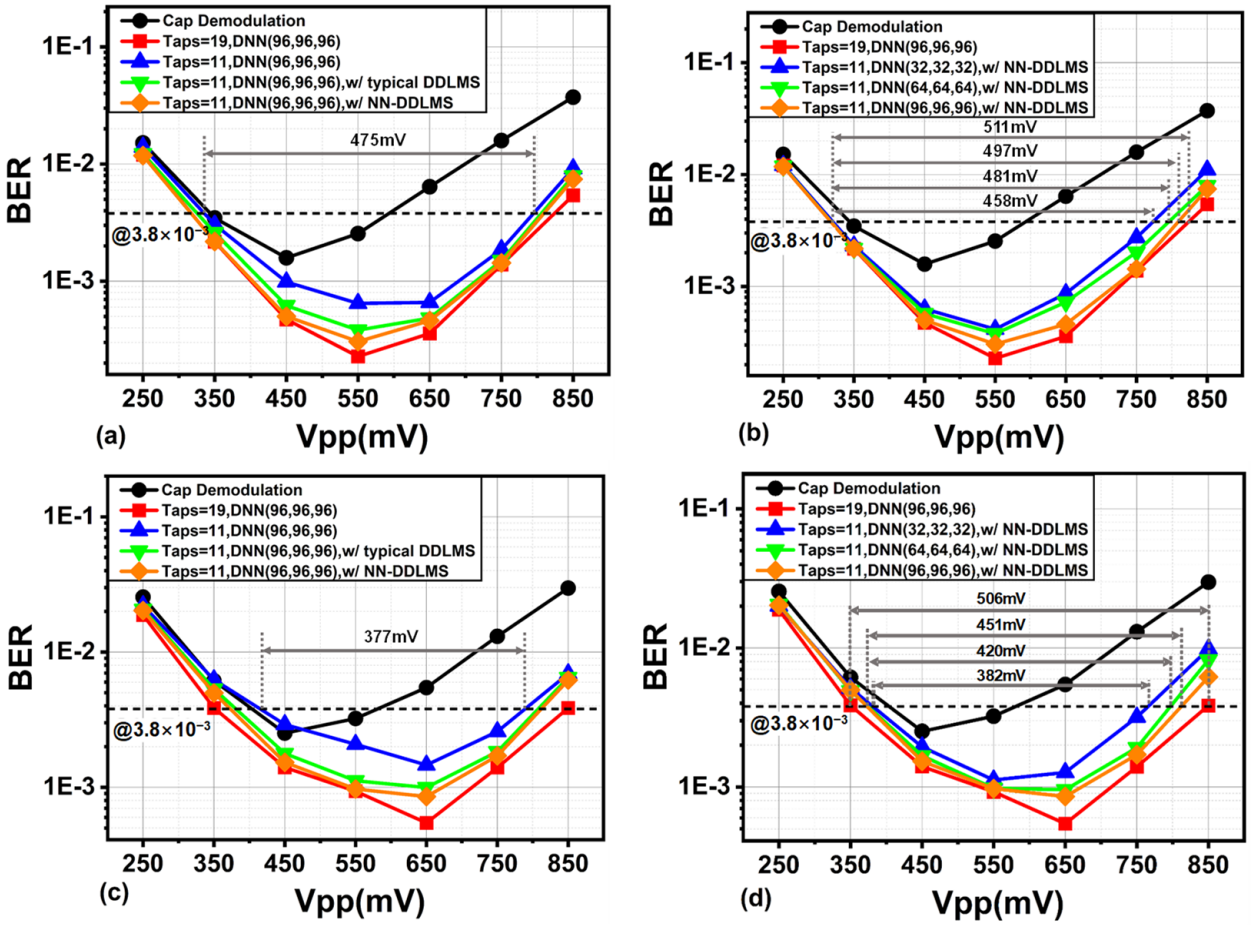

Figure 11. BER of different decoders versus different signal Vpp for (**a**) 64APSK; (**b**) 64APSK; (**c**) 64QAM; (**d**) 64QAM.

The BER performance and trainable parameters that represent the complexity of different receivers for 64APSK and 64QAM systems are compared in Tables 1 and 2, respectively. Ratio* represents the ratio between signal Vpp dynamic range (mV) and total trainable parameters. In Table 1, the traditional DNN converter we optimize, which points to DNN (96, 96, 96) with taps of 19, has a maximum signal Vpp dynamic range of 511 mV and maximum trainable parameters of 26,210 at the same time in 64APSK systems. In order to make a better tradeoff between communication performance and computation complexity, a cascaded receiver consisting of a DNN converter and NN-based DD-LMS is utilized. The complexity of a DNN converter varies greatly with the number of nodes, but that of NN-based DD-LMS is fixed at 84. As the nodes of each hidden layer reduce from 96 to 32, the dynamic range of the cascaded receiver slightly reduces from 497 mV to 458 mV (from 97.3% to 89.6% of maximum), but the complexity greatly reduces from 23,222 to 3702 (from 88.6% to 14.1% of maximum). The ratio of signal Vpp dynamic range and complexity increases from 2.14×10^{-2} mV to 1.24×10^{-1} mV, while that of traditional DNN converter is 1.95×10^{-2} mV. Notably, DNN (32, 32, 32) with NN-based DD-LMS

and taps of 11 could achieve 89.6% of signal Vpp dynamic range with 14.1% of complexity, which experimentally verifies the effectiveness of the proposed algorithm. It can be seen that the conclusions are similar in the 64QAM system in Table 2. However, the tradeoff between communication performance and computation complexity is worse than 64APSK. To be specific, as the nodes reduce from 96 to 32, the signal Vpp dynamic range reduces from 451 mV to 382 mV (from 89.1% to 75.5%), and the complexity greatly reduces from 23,222 to 3702 (from 88.6% to 14.1%). The ratio of signal Vpp dynamic range and complexity increases from 1.94×10^{-2} mV to 1.03×10^{-1} mV, while that of the traditional converter is 1.93×10^{-2} mV. Therefore, the proposed algorithm is experimentally validated to be an effective receiver to make a better tradeoff between communication performance and computation complexity than traditional DNN converter, especially in UVLC systems using 64APSK modulation format.

Table 1. Comparison of different receivers in 64APSK UVLC system.

Modulation Format	Network Structure	Trainable Parameters (DNN Converter)	Trainable Parameters (DD-LMS)	Total Trainable Parameters	Trainable Parameters Rate	Dynamic Range (mV)	Dynamic Range Rate	Ratio * (102 mV)
64APSK	Taps = 19, DNN (96, 96, 96) w/o NN DD-LMS	26,210	/	26,210	100%	511	100%	1.95
64APSK	Taps = 11, DNN (96, 96, 96) w/NN DD-LMS	23,138	84	23,222	88.6%	497	97.3%	2.14
64APSK	Taps = 11, DNN (64, 64, 64) w/NN DD-LMS	11,330	84	11,414	43.5%	481	94.1%	4.21
64APSK	Taps = 11, DNN (32, 32, 32) w/NN DD-LMS	3618	84	3702	14.1%	458	89.6%	12.4

Ratio * represents the ratio of dynamic range and trainable parameters.

Table 2. Comparison of different receivers in 64QAM UVLC system.

Modulation Format	Network Structure	Trainable Parameters (DNN Converter)	Trainable Parameters (DD-LMS)	Total Trainable Parameters	Trainable Parameters Ratio	Dynamic Range (mV)	Dynamic Range Ratio	Ratio * (102 mV)
64QAM	Taps = 19, DNN (96, 96, 96) w/o NN DD-LMS	26,210	/	26,210	100%	506	100%	1.93
64QAM	Taps = 11, DNN (96, 96, 96) w/NN DD-LMS	23,138	84	23,222	88.6%	451	89.1%	1.94
64QAM	Taps = 11, DNN (64, 64, 64) w/NN DD-LMS	11,330	84	11,414	43.5%	420	83.0%	3.68
64QAM	Taps = 11, DNN (32, 32, 32) w/NN DD-LMS	3618	84	3702	14.1%	382	75.5%	10.3

Ratio * represents the ratio of dynamic range and trainable parameters.

5. Conclusions

To alleviate bottleneck problems of high-speed underwater VLC systems, we construct and optimize a DNN-based waveform-to-symbol converter to replace conventional demodulation, down-sampling and post-equalization at the receiving end in 64APSK and 64QAM UVLC systems based on CAP modulation. The DNN converter optimizes the receiver as a whole rather than separately. It is regarded as a benchmark that could increase signal Vpp dynamic range by 104% (from 250 mV to 511 mV) for 64APSK and 181% (from 180 mV to 506 mV) for 64QAM with 7% FEC of 3.8×10^{-3} as a BER threshold, compared with traditional CAP decoder. The highest bit rate is 3.23 Gb/s in 64APSK systems utilizing the DNN converter we optimize and 3.09 Gb/s in 64QAM systems, which is 125 Mb/s

and 50 Mb/s faster than the traditional CAP decoder, respectively. However, it comes at the cost of high computation complexity of 26,210 total trainable parameters. To make a better tradeoff between communication performance and computation complexity, a cascaded receiver consisting of a DNN-based waveform-to-symbol converter and a modified NN-based DD-LMS algorithm is innovatively proposed. With fewer taps and nodes of hidden layers than the benchmark converter, the front-stage DNN converter could mitigate the majority of ISI and signal nonlinear distortions. Then modified NN-based DD-LMS is cascaded to improve communication performance by reducing phase offset, making received constellation points more concentrated and closer to standard constellation points. Compared with the benchmark converter, the cascade receiver could achieve 89.6% of the signal Vpp dynamic range with 12.4% of complexity or 94.1% of the signal Vpp dynamic range with 43.5% of complexity in the 64APSK UVLC system. Furthermore, the ratio of signal Vpp dynamic range and total trainable parameters is up to 1.24×10^{-1} mV, while that of the benchmark converter is 1.95×10^{-2} mV. The cascaded receiver used in 64APSK UVLC systems is experimentally validated to achieve enhanced performance between communication performance and computation complexity, regarded as a promising scheme for future high-speed underwater VLC.

Author Contributions: Conceptualization, X.L. and N.C.; methodology, X.L., F.H. and N.C.; software, X.L.; validation, X.L.; formal analysis, X.L.; investigation, X.L.; resources, X.L.; data curation, X.L.; writing—original draft preparation, X.L.; writing—review and editing, F.H. and N.C.; visualization, X.L.; supervision, N.C.; project administration, N.C.; funding acquisition, N.C. All authors have read and agreed to the published version of the manuscript.

Funding: This research was funded by the National Key Research and Development Program of China (2022YFB2802803), the Natural Science Foundation of China Project (No. 61925104, No. 62031011, No. 62201157) and Major Key Project of PCL.

Institutional Review Board Statement: Not applicable.

Informed Consent Statement: Not applicable.

Data Availability Statement: The data that support the findings of this study are available from the corresponding author upon reasonable request.

Conflicts of Interest: The authors declare no conflict of interest.

References

1. Oubei, H.M.; Li, C.; Park, K.-H.; Ng, T.K.; Alouini, M.-S.; Ooi, B.S. 2.3 Gbit/s underwater wireless optical communications using directly modulated 520 nm laser diode. *Opt. Express* **2015**, *23*, 20743–20748. [CrossRef]
2. Cossu, G.; Corsini, R.; Khalid, A.M.; Balestrino, S.; Coppelli, A.; Caiti, A.; Ciaramella, E. Experimental demonstration of high speed underwater visible light communications. In Proceedings of the 2013 2nd International Workshop on Optical Wireless Communications (IWOW), Newcastle Upon Tyne, UK, 21–21 October 2013; pp. 11–15.
3. Wang, C.; Yu, H.Y.; Zhu, Y.J. A Long Distance Underwater Visible Light Communication System with Single Photon Avalanche Diode. *IEEE Photonics J.* **2016**, *8*, 7906311. [CrossRef]
4. O'Brien, D.; Le Minh, H.; Zeng, L.; Faulkner, G.; Lee, K.; Jung, D.; Oh, Y.; Won, E.T. Indoor visible light communications: Challenges and prospects. *Free-Space Laser Commun. VIII* **2008**, *7091*, 60–68.
5. Chi, N.; Haas, H.; Kavehrad, M.; Little, T.D.C.; Huang, X.L. Visible light communications: Demand factors, benefits and opportunities [Guest Editorial]. *IEEE Wirel. Commun.* **2015**, *22*, 5–7. [CrossRef]
6. Chi, N.; Zhou, Y.; Liang, S.; Wang, F.; Li, J.; Wang, Y. Enabling Technologies for High-Speed Visible Light Communication Employing CAP Modulation. *J. Light. Technol.* **2018**, *36*, 510–518. [CrossRef]
7. Zhou, Y.; Zhu, X.; Hu, F.; Shi, J.; Wang, F.; Zou, P.; Liu, J.; Jiang, F.; Chi, N. Common-anode LED on a Si substrate for beyond 15Gbit/s underwater visible light communication. *Photon. Res.* **2019**, *7*, 1019–1029. [CrossRef]
8. Huang, X.; Wang, Z.; Shi, J.; Wang, Y.; Chi, N. 1.6 Gbit/s phosphorescent white LED based VLC transmission using a cascaded pre-equalization circuit and a differential outputs PIN receiver. *Opt. Express* **2015**, *23*, 22034–22042. [CrossRef]
9. Haigh, P.A.; Burton, A.; Werfli, K.; Le Minh, H.; Bentley, E.; Chvojka, P.; Popoola, W.O.; Papakonstantinou, I.; Zvanovec, S. A multi-CAP visible-light communications system with 4.85-b/s/Hz spectral efficiency. *IEEE J. Sel. Areas Commun.* **2015**, *33*, 1771–1779. [CrossRef]
10. Cossu, G.; Khalid, A.; Choudhury, P.; Corsini, R.; Ciaramella, E. 3.4 Gbit/s visible optical wireless transmission based on RGB LED. *Opt. Express* **2012**, *20*, B501–B506. [CrossRef]

11. Wang, Y.; Huang, X.; Zhang, J.; Wang, Y.; Chi, N. Enhanced performance of visible light communication employing 512-QAM N-SC-FDE and DD-LMS. *Opt. Express* **2014**, *22*, 15328–15334. [CrossRef]
12. Zhao, J.; Qin, C.; Zhang, M.; Chi, N. Investigation on performance of special-shaped 8-quadrature amplitude modulation constellations applied in visible light communication. *Photonics Res.* **2016**, *4*, 249–256. [CrossRef]
13. Yan, K.; Yang, F.; Song, J.; Ren, F.; Li, J. A framework of APSK constellation labeling design for satellite transmission. In Proceedings of the 2014 IEEE International Conference on Communications (ICC), Sydney, NSW, Australia, 10–14 June 2014; pp. 4337–4341.
14. CCSDS. Flexible Advanced Coding and Modulation Scheme for High Rate Telemetry Applications. 2012. Available online: https://cwe.ccsds.org/sls/docs/SLS-CandS/Meeting%20Public%20Materials/2011/201110.Boulder/131.2-R-2.SCC-Review/DispositionsFinalized/131x2r2[underReview-20111103].pdf (accessed on 10 December 2022).
15. Stepniak, G.; Siuzdak, J.; Zwierko, P. Compensation of a VLC phosphorescent white LED nonlinearity by means of Volterra DFE. *IEEE Photonics Technol. Lett.* **2013**, *25*, 1597–1600. [CrossRef]
16. Wang, Y.; Huang, X.; Tao, L.; Shi, J.; Chi, N. 4.5-Gb/s RGB-LED based WDM visible light communication system employing CAP modulation and RLS based adaptive equalization. *Opt. Express* **2015**, *23*, 13626–13633. [CrossRef]
17. Huang, X.; Shi, J.; Li, J.; Wang, Y.; Chi, N. A Gb/s VLC Transmission Using Hardware Preequalization Circuit. *IEEE Photonics Technol. Lett.* **2015**, *27*, 1915–1918. [CrossRef]
18. Zhang, G.; Zhang, J.; Hong, X.; He, S. Low-complexity frequency domain nonlinear compensation for OFDM based high-speed visible light communication systems with light emitting diodes. *Opt. Express* **2017**, *25*, 3780–3794. [CrossRef]
19. Chi, N.; Zhao, Y.; Shi, M.; Zou, P.; Lu, X. Gaussian kernel-aided deep neural network equalizer utilized in underwater PAM8 visible light communication system. *Opt. Express* **2018**, *26*, 26700–26712. [CrossRef]
20. Lu, X.; Lu, C.; Yu, W.; Qiao, L.; Liang, S.; Lau, A.P.T.; Chi, N. Memory-controlled deep LSTM neural network post-equalizer used in high-speed PAM VLC system. *Opt. Express* **2019**, *27*, 7822–7833. [CrossRef] [PubMed]
21. Chen, H.; Zhao, Y.; Hu, F.; Chi, N. Nonlinear Resilient Learning Method Based on Joint Time-Frequency Image Analysis in Underwater Visible Light Communication. *IEEE Photonics J.* **2020**, *12*, 7901610. [CrossRef]
22. Chen, J.; Wang, Z.; Zhao, Y.; Zhang, J.; Li, Z.; Shen, C.; Chi, N. Neural Network Detection for Bandwidth-Limited Non-Orthogonal Multiband CAP UVLC System. *IEEE Photonics J.* **2022**, *14*, 7322309. [CrossRef]
23. Chen, J.; Jia, J.; Xing, S.; Wang, J.; Shi, J.; Zhang, J.; Chi, N. Neural-network-based direct waveform to symbol conversion for joint ISI and ICI cancellation in non-orthogonal multi-band CAP based UDWDM fiber-mmWave integration. *Opt. Express* **2022**, *30*, 35684–35697. [CrossRef]
24. Cai, J.; Xu, Z.; Chi, N. Constellation Shaping and AI-Driven Demodulation Techniques in Visible Light Communication. *ZTE Technol. J.* **2022**, *28*, 19–24.
25. Zhao, Y.; Zou, P.; Yu, W.; Chi, N. Two tributaries heterogeneous neural network based channel emulator for underwater visible light communication systems. *Opt. Express* **2019**, *27*, 22532–22541. [CrossRef] [PubMed]
26. Li, Z.; Shi, J.; Zhao, Y.; Li, G.; Chen, J.; Zhang, J.; Chi, N. Deep learning based end-to-end visible light communication with an in-band channel modeling strategy. *Opt. Express* **2022**, *30*, 28905–28921. [CrossRef]
27. Li, L.; Zhu, Z.; Zhang, J. Neural Network-Based Transceiver Design for VLC System over ISI Channel. *Photonics* **2022**, *9*, 190. [CrossRef]
28. Rodes, R.; Wieckowski, M.; Pham, T.T.; Jensen, J.B.; Turkiewicz, J.; Siuzdak, J.; Monroy, I.T. Carrierless amplitude phase modulation of VCSEL with 4 bit/s/Hz spectral efficiency for use in WDM-PON. *Opt. Express* **2011**, *19*, 26551–26556. [CrossRef] [PubMed]
29. Wieckowski, M.; Jensen, J.B.; Monroy, I.T.; Siuzdak, J.; Turkiewicz, J.P. 300 Mbps Transmission with 4.6 bit/s/Hz Spectral Efficiency over 50 m PMMA POF Link Using RC-LED and Multi-Level Carrierless Amplitude Phase Modulation. In Proceedings of the Optical Fiber Communication Conference/National Fiber Optic Engineers Conference 2011, Los Angeles, CA, USA, 6 March 2011; p. NTuB8.
30. Ye, H.; Li, G.Y.; Juang, B.H. Power of Deep Learning for Channel Estimation and Signal Detection in OFDM Systems. *IEEE Wirel. Commun. Lett.* **2018**, *7*, 114–117. [CrossRef]